Electronic Supplementary Information for Experimentally Probing the Libration of Interfacial Water: the Rotational Potential of Water is Stiffer at the Air/Water Interface than in Bulk Liquid

Yujin Tong, Tobias Kampfrath, and R. Kramer Campen*

Fritz Haber Institute of the Max Planck Society, Faradayweg 4-6, 14195 Berlin, Germany

E-mail: campen@fhi-berlin.mpg.de

Phone: +49 (0)30 8413-5230. Fax: +49 (0)30 8413-5106

1 Details of our VSF Spectrometer and Sample

The VSF spectrometer used in this work consists of a mode-locked Ti:Sapphire Oscillator (Venteon), a regenerative amplifier and a subsequent cryo-cooled amplifier (Coherent). The amplifier delivers 800 nm, 35 fs, 15 mJ pulses at a repetition rate of 1 kHz. Half of this energy is used to generate infrared pulses centered at 12 μm ($\approx$ 833 cm^{-1}) by difference frequency mixing of the signal and idler output of a commercial optical parametric amplifier (TOPAS, Light Conversion). The residual of the 800 nm light from the parametric amplification is spectrally narrowed using a home-made pulse shaper – composed of a grating, mirror and

*To whom correspondence should be addressed

slit combination – and used as the up conversion field in the sum frequency process (*i.e.* the *visible* field in the usual VSF terminology). The spectral width of the visible pulse is set to < 2 nm. For all measurements, the energy per pulse of the infrared at the sample surface was 6.0 μJ, and that of the visible 18 μJ. The infrared and visible beams were focused on the samples by lenses with focal length of 10 and 35 cm, and , as noted in the text, had incident angles of $55\pm1^\circ$ and $65\pm1^\circ$ for geometry I and $60\pm1^\circ$ and $40\pm1^\circ$ for geometry II. The size of the infrared and visible foci at the sample were 80 and 200 μm respectively. After the sample, the VSF signal was collimated by a lens (f=450 mm) and focused again on the entrance slit of a spectrograph (Andor technology, Shamrock 303). Finally, the dispersed signals were imaged on an EMCCD camera (Andor, Newton).

Our spectrograph was calibrated using emission lines from a Neon lamp; the frequency calibration of the spectrum was performed using a polystyrene thin film and relative VSF intensities in different experimental geometries were quantitatively compared using the resonant signal from z-cut quartz as a reference. To account for the frequency-dependent IR pulse energy, we normalized the measured VSF response from the air/H_2O interface by the, nonresonant, VSF signal from a gold mirror. The acquisition time for measurements of the VSF spectral response of the gold mirror and H_2O were 30 and 600 seconds, respectively.

H_2O measurements were carried out in a home built teflon trough using Millipore MilliQ (resistivity > 18.2 M$\Omega \cdot$ cm) water.

2 Quantitatively Comparing $\mathbf{I_{VSF}}$ Collected in Different Experimental Geometries

2.1 Quantifying Reflected $\mathbf{I_{VSF}}$

As discussed in detail by prior authors,[1–3] given an interface irradiated by optical fields at infrared (E_{IR}) and visible (E_{VIS}) frequencies, and describing the system in the electric dipole

approximation, a second order nonlinear polarization is generated in the interfacial layer which radiates in the reflected direction,

$$I_{\mathrm{VSF}} = \frac{8\pi\nu_{\mathrm{VSF}}^3 \sec^2\theta_{\mathrm{VSF}}}{c^3} \left| E_{\mathrm{VIS}}(\nu_{\mathrm{VIS}}) \otimes \chi_{\mathrm{eff}}^{(2)} \right|^2 I_{\mathrm{IR}}(\nu_{\mathrm{IR}}) \tag{1}$$

in which E_{VIS} is the, frequency dependent, 800 nm field, $\otimes$ is the convolution operator, $\chi_{\mathrm{eff}}^{(2)}$ is the effective macroscopic second order nonlinear susceptibility, θ_{VSF} is the angle at which the sum frequency emission radiates and I_{IR} is the, frequency dependent, infrared intensity.

$\chi_{\mathrm{eff}}^{(2)}$ is a function of both the intrinsic, second-order response of the material $\chi^{(2)}$, the polarizations of the incident and outgoing fields, and the Fresnel coefficients. It can be expressed, most generally, as (in which $\hat{e}$ is the unit polarization vector of the indicated beams),

$$\chi_{\mathrm{eff}}^{(2} = [\hat{e}_{\mathrm{VSF}} \cdot \boldsymbol{L}_{\mathrm{VSF}}] \cdot \chi^{(2)}(\nu_{IR}) : [\hat{e}_{\mathrm{VIS}} \cdot \boldsymbol{L}_{\mathrm{VIS}}][\hat{e}_{\mathrm{IR}} \cdot \boldsymbol{L}_{\mathrm{IR}}] \tag{2}$$

As described in the manuscript, we fit the data by substituting equation (2) into (1).

For interfaces, such as the air/water, that have macroscopic $C_{\infty\nu}$ symmetry, there are four independent, nonzero components of $\chi^{(2)}$. Given the experimental geometry shown in the manuscript, z is the surface normal and all fields propagate in the x-z plane, these nonzero components are, $\chi_{xxz}^{(2)} = \chi_{yyz}^{(2)}$, $\chi_{xzx}^{(2)} = \chi_{yzy}^{(2)}$, $\chi_{zxx}^{(2)} = \chi_{zyy}^{(2)}$ and $\chi_{zzz}^{(2)}$. Measuring I_{VSF} under the *ssp* and *ppp* polarization conditions (in which *s* indicates a field perpendicular to the x-z plane and *p* parallel) samples these nonzero components of the $\chi^{(2)}$,

$$\chi_{\mathrm{eff},ssp}^{(2)} = L_{yy}(\nu_{\mathrm{VSF}}) L_{yy}(\nu_{\mathrm{VIS}}) L_{zz}(\nu_{\mathrm{IR}}) \sin\theta_{\mathrm{IR}} \chi_{yyz}^{(2)} \tag{3}$$

$$\begin{aligned} \chi_{\mathrm{eff},ppp}^{(2)} = & -L_{xx}(\nu_{\mathrm{VSF}}) L_{xx}(\nu_{\mathrm{VIS}}) L_{zz}(\nu_{\mathrm{IR}}) \cos\theta_{\mathrm{VSF}} \cos\theta_{\mathrm{VIS}} \sin\theta_{\mathrm{IR}} \chi_{xxz}^{(2)} \\ & -L_{xx}(\nu_{\mathrm{VSF}}) L_{zz}(\nu_{\mathrm{VIS}}) L_{xx}(\nu_{\mathrm{IR}}) \cos\theta_{\mathrm{VSF}} \sin\theta_{\mathrm{VIS}} \cos\theta_{\mathrm{IR}} \chi_{xzx}^{(2)} \\ & +L_{zz}(\nu_{\mathrm{VSF}}) L_{xx}(\nu_{\mathrm{VIS}}) L_{xx}(\nu_{\mathrm{IR}}) \sin\theta_{\mathrm{VSF}} \cos\theta_{\mathrm{VIS}} \cos\theta_{\mathrm{IR}} \chi_{zxx}^{(2)} \\ & +L_{zz}(\nu_{\mathrm{VSF}}) L_{zz}(\nu_{\mathrm{VIS}}) L_{zz}(\nu_{\mathrm{IR}}) \sin\theta_{\mathrm{VSF}} \sin\theta_{\mathrm{VIS}} \sin\theta_{\mathrm{IR}} \chi_{zzz}^{(2)} \end{aligned} \tag{4}$$

in which θ_i is the angle of the ith field with respect to the surface normal and $L_{jj}(\Omega)$ are the diagonal elements of the Fresnel factors evaluated at frequency Ω. The diagonal elements of the Fresnel factor are given,

$$L_{xx}(\Omega) = \frac{2\cos\gamma}{\cos\gamma + n_{\mathrm{H_2O}}(\Omega)\cos\theta_i} \quad (5)$$

$$L_{yy}(\Omega) = \frac{2\cos\theta_i}{\cos\theta_i + n_{\mathrm{H_2O}}(\Omega)\cos\gamma} \quad (6)$$

$$L_{zz}(\Omega) = \frac{2n_{\mathrm{H_2O}}(\Omega)\cos\theta_i}{\cos\gamma + n_{\mathrm{H_2O}}(\Omega)\cos\theta_i}\left(\frac{1}{n'(\Omega)}\right)^2 \quad (7)$$

in which $n_{\mathrm{H_2O}}(\Omega)$ is the refractive index of water at frequency Ω, θ_i is the angle of incidence of the i^{th} beam (either IR, VIS or VSF), γ is the refraction angle (*i.e.* $\sin\theta_i = n_{\mathrm{H_2O}}(\Omega)\sin\gamma$) and $n'(\Omega)$ is the interfacial refractive index at frequency Ω. The interfacial refractive index for this system is calculated using the approach described by Shen and coworkers.[1]

The solutions to equations (5), (6) and (7) for our experimental Geometries I and II are shown in Figure S1. The effect of the frequency dependent refractive index of water is apparent in both figures. Clearly one needs to account for this frequency dependence in the linear optical response to extract the true, frequency dependent, $\chi^{(2)}$. Additionally inspection of the Fresnel coefficients for Geometry 2 in the *ppp* polarization condition highlights that the frequency dependence of the Fresnel coefficients of each of the components of $\chi^{(2)}$ that contribute to the signal differ dramatically. Clearly accounting for these effects is important in recovering the true sum frequency spectral response. As is clear from the lineshape equations given in the text, spectra measured under the *ppp* polarization condition are a, nontrivial, product of the xxz, xzx, zxx and zzz terms.

2.2 Normalization to Account for the IR Spectral Profile

Our infrared source strongly varies in power as a function of frequency. To account for this variation, as discussed in the text, we measure the I_{VSF} emitted from a Au mirror at the

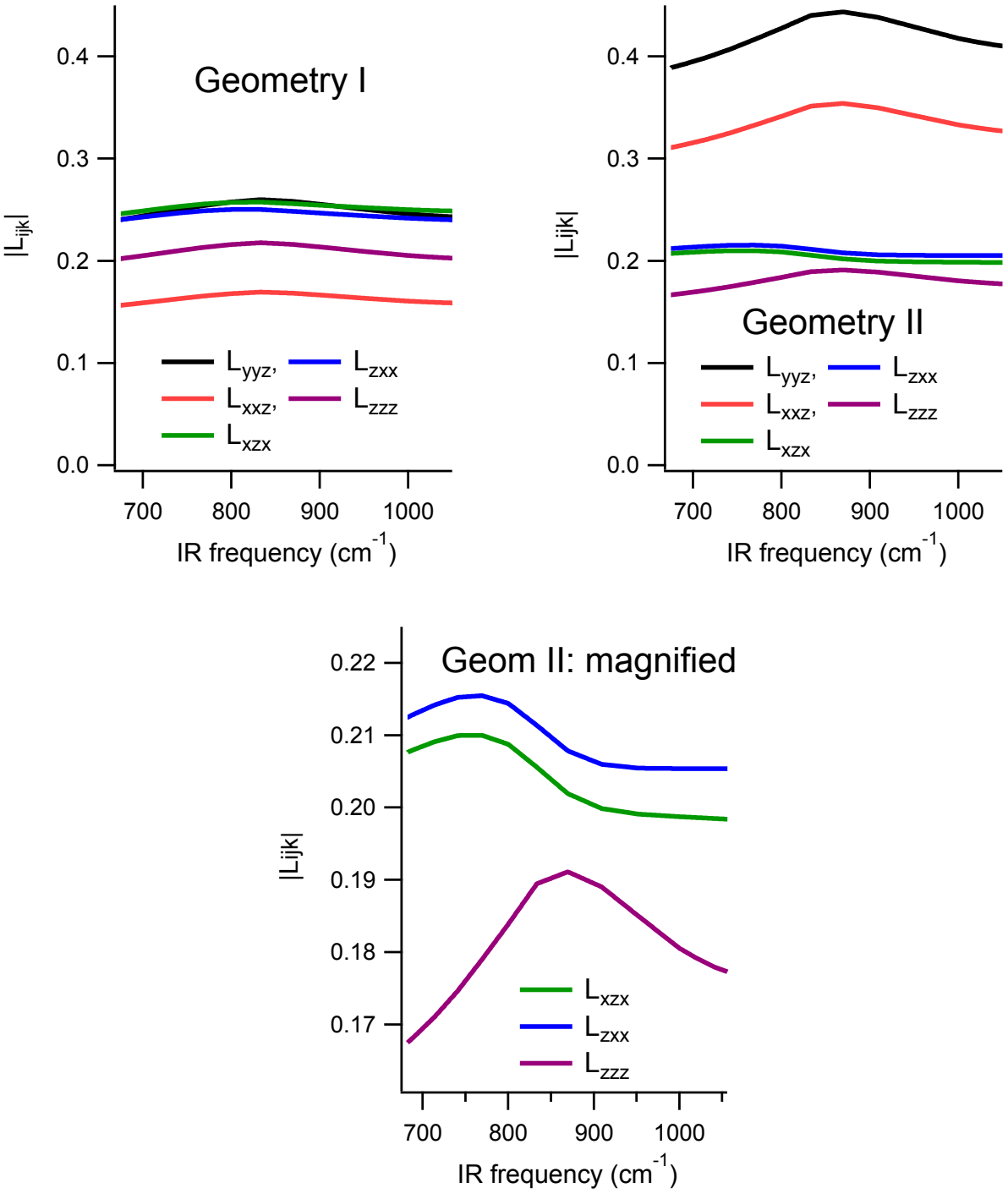

Figure S1: Frequency dependent Fresnel coefficients for the air/H_2O interface employing the incident angles in geometry I (left panel) and those in geometry II (right and bottom panels). For brevity, the product $L_{ii}(\nu_{\mathrm{VSF}})L_{jj}(\nu_{\mathrm{VIS}})L_{kk}(\nu_{\mathrm{IR}})$ has been abbreviated L_{ijk}.

same location as the sample. Because Au has no resonances in our frequency range of interest $\chi^{(2)} = \chi^{(2)}_{\rm nr}$. As changes in the refractive index of Au are small over our wavelength ranges of interest, the measured $I_{\rm VSF}$ is dominated by changes in $I_{\rm IR}$.

2.3 Normalization Procedure to Between Experimental Geometries

Changing incident beam angles may result in a variety of, unintended, changes in the experimental set up that may make quantitative comparison of sum frequency intensities challenging: spatial and temporal overlap of the two beams may slightly change, the alignment of the detected sum frequency with respect to the spectrometer may change, etc. As mentioned in the text we quantitatively corrected for such, inadvertent differences in the experimental set up by using z-cut quartz as a reference. The approach is as follows:

1. We calculated the frequency dependent Fresnel coefficients, *i.e.* equations 5-7 and the coherence length in z-cut quartz for our two experimental geometries (as shown in Figures S2 and S3).

2. Z-cut quartz has three resonances in our frequency range of interest. Assuming a Lorentzian line shape and employing the fit parameters for each resonance previously published by Shen and coworkers[4] we calculated the $\chi^{(2)}_r$. This result is shown in Figure S4 and is independent of the incident beam angles.

3. Armed with this information we calculated the expected change in $I_{\rm sf}$ with changes in experimental geometry (see Figure S5). As shown in Figure S6 the calculated trends in resonance amplitude as a function of geometry are fairly well reproduced in experiment (given the finite spectral resolution in our experimental configuration much of the fine spectral detail is lost).

4. Following this procedure showed a mismatch between experiment and calculation of 5%: it was necessary to divide the $\chi^{(2)}_{ijk}$ extracted from Geometry II by 1.05 to recover the expected value relative to $\chi^{(2)}_{ijk}$ in Geometry I.

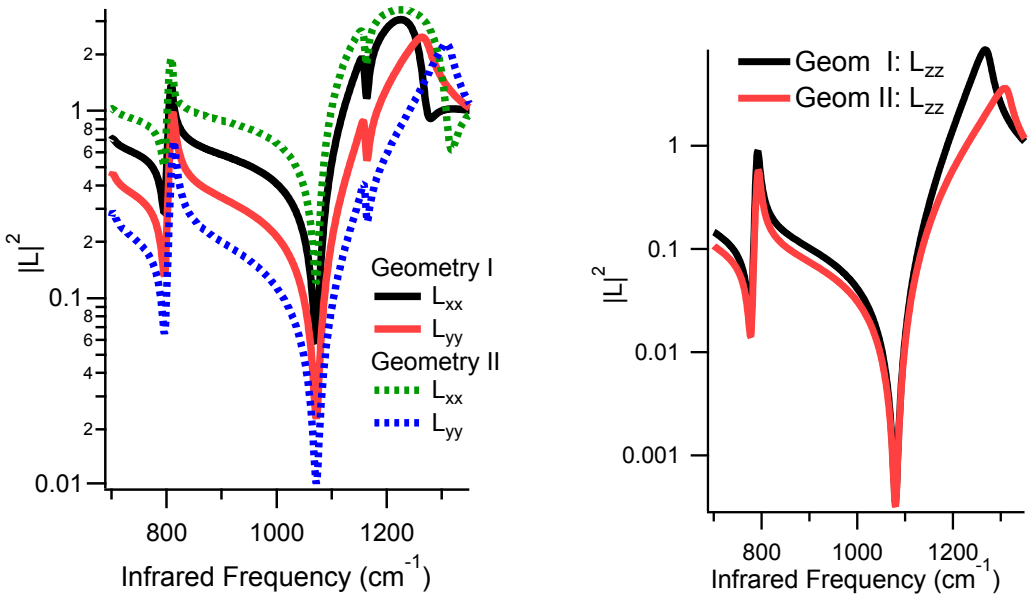

Figure S2: Frequency dependent Fresnel coefficients for z-cut quartz under different experimental geometries.

The error captured in this correction factor is independent of all quartz properties. Thus we expect it also to apply when changing experimental geometries on the water surface. All reported VSF spectra of the water surface in Geometry II have thus been divided by 1.05. In any case, as is clear from inspection of the data in the paper, all conclusions are insensitive to this correction.

3 Control Experiments

We determined that our sample was contaminant-free, *i.e.* that the signal we observe is a property of interfacial H_2O, by collecting spectra at CH stretch (no CH signal was apparent) and OH stretch (the VSF spectra was quantitatively the same as published reports with our sample preparation procedure) frequencies at the air/H_2O interface. In addition we also collected spectra at librational frequencies at the air/D_2O interface.

In infrared absorption measurements the center frequency of the rotational libration

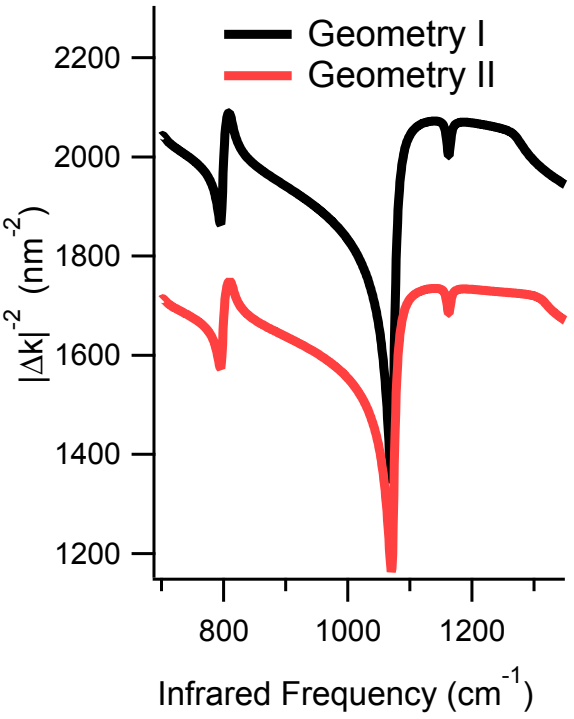

Figure S3: Calculated, frequency dependent, wavevector mismatch of the visible and infrared beams in z-cut quartz as a function of experimental geometry.

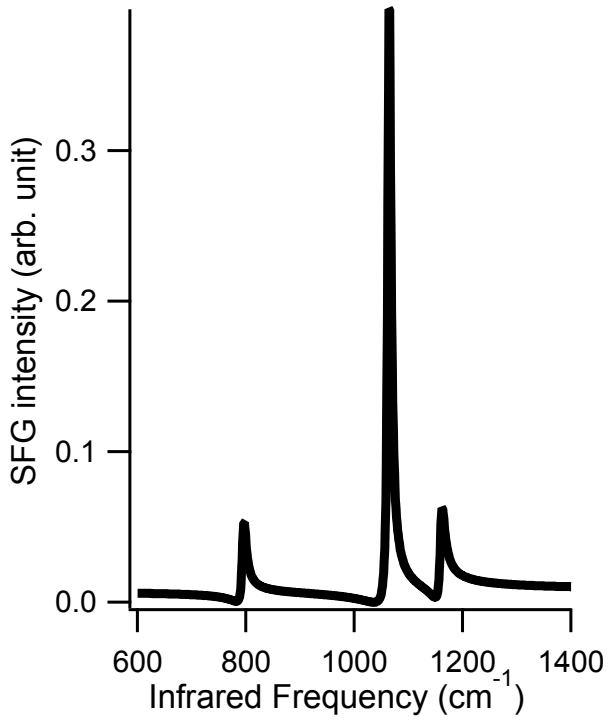

Figure S4: Calculated frequency dependent $\chi^{(2)}_{aaa}$ of quartz using the parameters of Liu and Shen.[4]

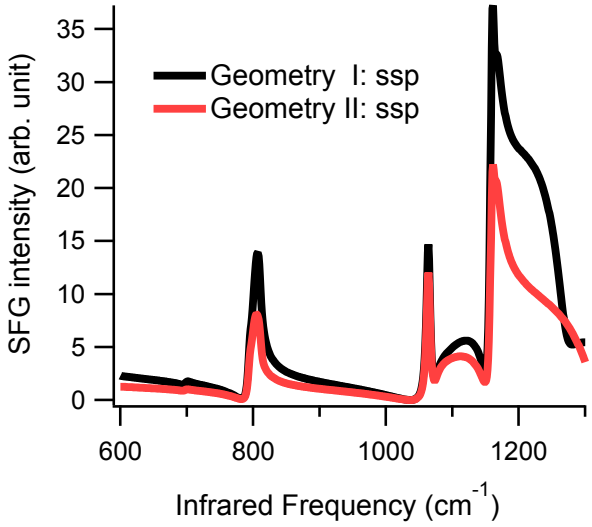

Figure S5: Calculated sum frequency intensity from α-quartz as a function of experimental geometry using the results shown in Figures S2, S3 and S4. Note the change in resonance intensity as a function of experimental geometry. This signal assumes that spectral resolution is not limited by the width of the visible pulse or gratings in the spectrometer.

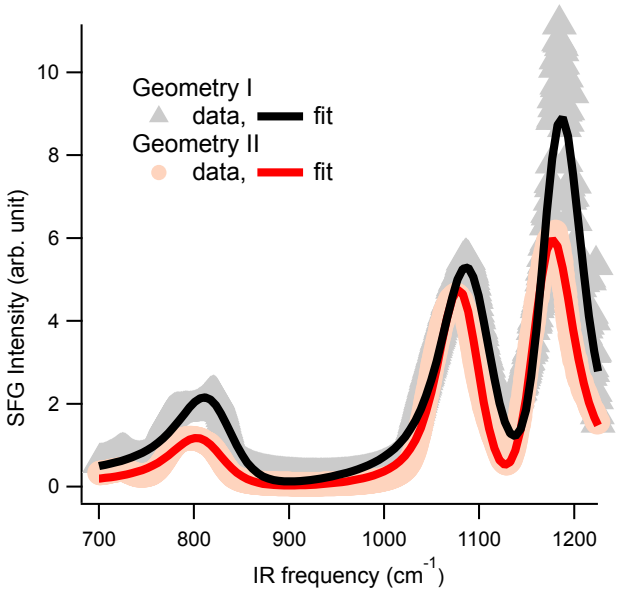

Figure S6: Measured I_{sf} from α-quartz in experimental geometry 1 and 2. All spectra are measured under the *ssp* polarization condition. As is clear from comparison with Figure S5 the modulation of resonance amplitude with changing beam incident angles is well predicted by the calculation. The measured data is considerably lower resolution owing the spectral width of the visible pulse.

spectral response in D_2O is red shifted by ≈ 170 cm^{-1} relative to H_2O: 500 v. 670 cm^{-1}.[5] Many prior studies have shown that in the bond stretch frequency range the IR absorption spectra of D_2O can be quantitatively related to that of H_2O by accounting for the effect of the change of mass on the force constant. A similar relationship has been shown to exist for the VSF spectra of the OD and OH stretch at the air/D_2O and air/H_2O interface respectively.[3,6] It therefore seems reasonable to suggest that, whatever its precise value, the interfacial rotational libration at the air/D_2O interface should be substantially red-shifted from that at the air/H_2O. Indeed, as shown in Figure S7, this is what we observe and no modes characteristic of, for example, multicarbon organic compounds, are apparent.

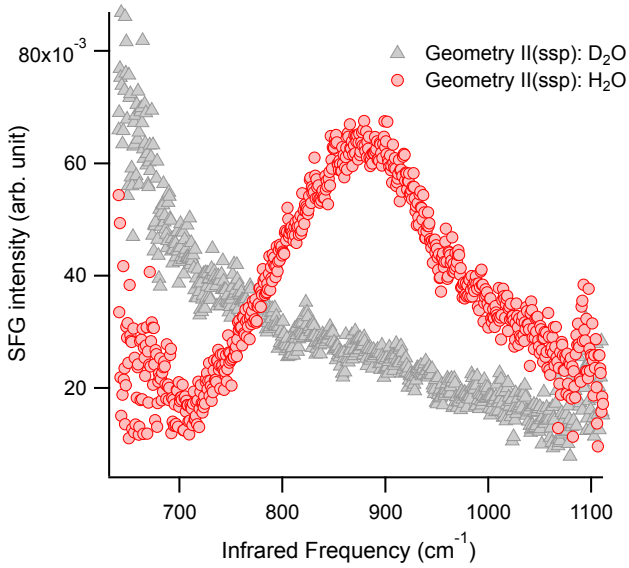

Figure S7: VSF spectral response as a function of infrared frequency for the water librational modes, in Geometry 2 (incident angles of 40° and 60° for the visible and infrared) under the *ssp* polarization condition.

We determined that the signal we observed was, in fact, a sum frequency signal, by its energy (we detected it at the sum of the frequencies of the VIS and IR fiels), its direction (it was detectable only at the expected angle dictated by phase matching) and its power dependence (the measured signal varied linearly with both incident IR and VIS intensities.

4 Details of Quantitative Line Shape Analysis

4.1 Is a Resonance Required to Fit the Data?

Because the linear refractive index of water changes significantly over our frequency range of interest it is possible an apparent frequency dependent I_{VSF} may simply be the result of a nonresonant response multiplied by the, frequency dependent, Fresnel coefficients. Using the line shape model described in the manuscript, equations (5)-(7), treating all nonresonant amplitudes as free parameters and assuming $\chi_r^{(2)} = 0$ we calculated the frequency dependent I_{VSF} shown in Figure S8. Clearly we cannot reproduce the data with $\chi_r^{(2)} = 0$: the apparent center frequencies, spectral amplitudes and changes in intensity with polarization and incident beam angle do not reproduce the data.

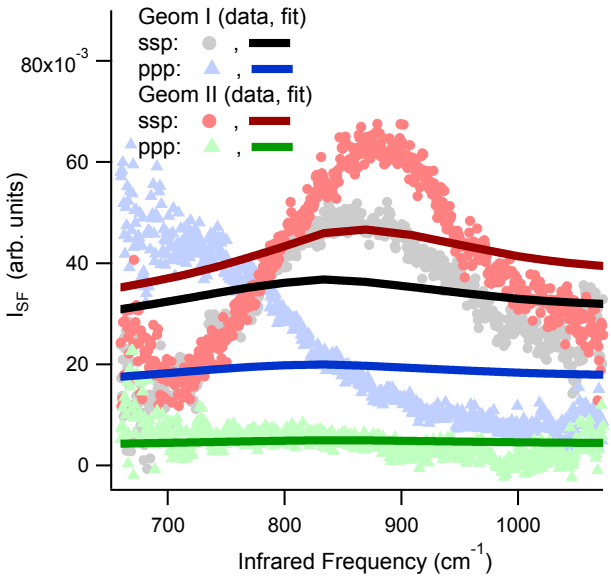

Figure S8: Calculated sum frequency intensity assuming that $\chi_r^{(2)} = 0$. Clearly the data cannot be reproduced with this assumption.

4.2 Quantifying the Resonant Spectral Response

Quantifying the observed line shape using the model described in the text is an underdetermined problem: we are unable to invert from the data to a unique amplitude (tensor component dependent), line width and center frequency for the observed resonance. However, fitting the data using a variety of assumptions about the resonant response illustrates that while the spectral amplitude ascribed to a particular $\chi^{(2)}$ component depends sensitively on assumptions the center frequency and line width are relatively insensitive.

In Table S1 we show a global fit to the data from both experimental geometries assuming that $\chi_{nr,xxz} = \chi_{nr,xzx} = \chi_{nr,zxx} = \chi_{nr,zzz}$, $\epsilon_{xxz} = \epsilon_{xzx} = \epsilon_{zxx} = \epsilon_{zzz}$: the nonresonant amplitude and phase are the same for all components of $\chi^{(2)}_{nr}$ that contribute to the $\chi^{(2)}_{\text{eff},ppp}$.

Table S1: Fit parameters for the fits to the data shown in the manuscript. Values of ϵ are given in radians. Values of Γ and $\tilde{\nu}$ are in cm^{-1}, values of $\chi_{nr,ijk}$ are in $10^{-21}\frac{mC\cdot cm}{V^2 sec}$ and χ_{ijk} are in $10^{-21}\frac{mC}{V^2 sec}$.

$\chi_{nr,yyz} =$	-0.33 ± 0.02
$\epsilon_{yyz} =$	2.07 ± 0.06
$2\Gamma_{\text{vis}} =$	37
$\chi_{yyz} = \chi_{xxz} =$	75.7 ± 5.2
$\tilde{\nu} =$	832 ± 3
$\Gamma =$	135 ± 3
$\chi_{nr,xxz} = \chi_{nr,xzx} = \chi_{nr,zxx} = \chi_{nr,zzz} =$	0.19 ± 0.003
$\epsilon_{xxz} = \epsilon_{xzx} = \epsilon_{zxx} = \epsilon_{zzz} =$	1.99 ± 0.01
$\chi_{xzx} =$	-66.4 ± 97.5
$\chi_{zxx} =$	-220 ± 138
$\chi_{zzz} =$	439 ± 164

4.3 Can the center frequency of our observed resonance be significantly red shifted?

As discussed above, unambiguously fitting our observed spectral response is extremely challenging. Particularly in light of the computational study of Nagata and coworkers,[7] it is reasonable to ask whether our observations would be consistent with a scenario in which the center frequency of the underlying resonance was at 670 cm^{-1} with a FWHM of 360 cm^{-1}

(*i.e.* the line shape of the bulk rotational libration at room temperature determined by Zelsmann and coworkers[5]) and the intensity maximum observed under the *ssp* polarization condition was shifted to 870 cm^{-1} due to a large nonresonant amplitude and appropriate nonresonant phase. In Figure S9, assuming the indicated resonant center frequency and damping constant, the dependence of the resulting sum frequency emission on nonresonant phase is illustrated. This comparison clearly demonstrates that $\epsilon = 0$ is required to move the resulting signal towards our observation. Assuming then, a resonant center frequency of 670 cm^{-1}, a resonant FWHM of 360 cm^{-1} and a nonresonant phase (*i.e.* ϵ) of 0, Figure S10 shows the expected signal as a ratio of nonresonant to resonant amplitude (*i.e.* $\chi_{nr,ijk}/\chi_{ijk}$ and compares these results with our data. Clearly it is not possible to shift the resonance sufficiently to reproduce our data and attempting to do so results in spectral distortions, *e.g.* a large apparent baseline, that are not observed.

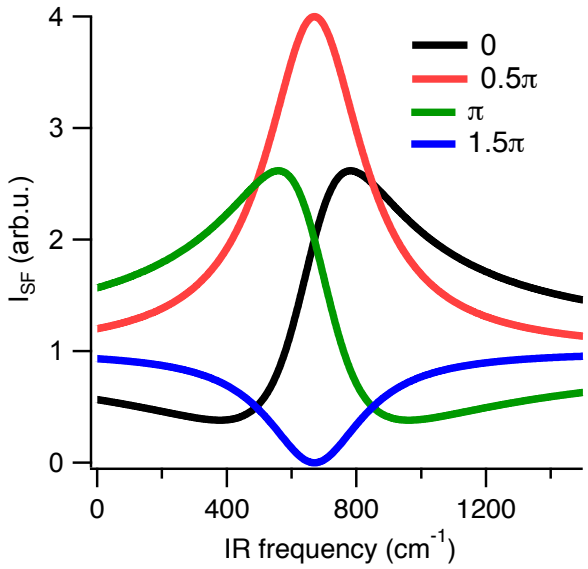

Figure S9: Calculated I_{sf} assuming a single resonance with center frequency 670 cm^{-1} and FWHM of 360 cm^{-1}, $\chi_{nr,ijk} = \chi_{ijk}/\Gamma$ and different values of ϵ as indicated. Clearly $\epsilon = 0$ most efficiently shifts the maximum measured I_{sf} to higher frequencies.

We have analyzed our data assuming $\chi_{nr,ijk} << \chi_{ijk}$ as has been shown to be the case for higher frequency modes of interfacial water. To our knowledge there is no physical mechanism

that would invalidate this relationship over our frequency range of interest (750-1050 cm^{-1}). Clearly slight deviations from this relationship would make it possible to describe our data with resonance frequencies that are somewhat lower that reported in Table S1. Nevertheless, as demonstrated in Figures S9 and S10 such a resonance would still be considerably higher energy than the rotational libration in bulk, thus demonstrating the essential insensitivity of our conclusions to this point.

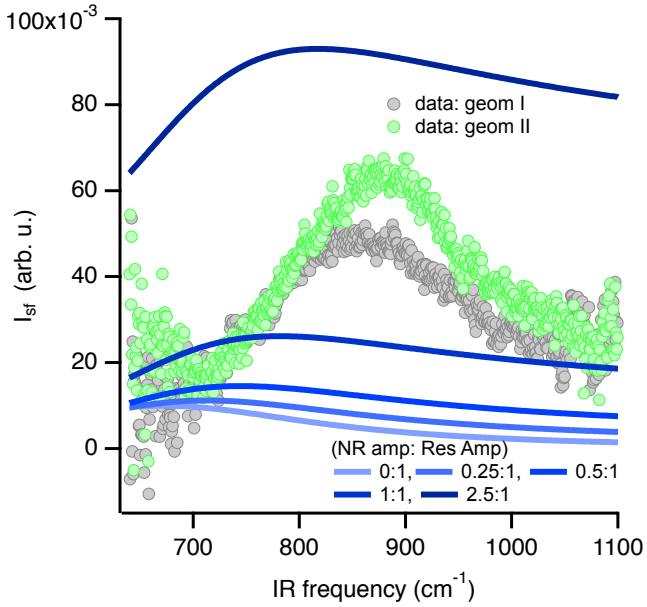

Figure S10: Calculated signal assuming resonant center frequency is 670 cm^{-1} with a FWHM of 360 cm^{-1}, $\epsilon = 0$ and the $\chi_{nr,ijk}/\chi_{ijk}$ ratio indicated. Experimental VSF spectra measured under the *ssp* polarization condition are plotted for comparison as measured in the indicated geometry.

References

(1) Zhuang, X.; Miranda, P. B.; Kim, D.; Shen, Y. R. *Phys. Rev. B* **1999**, *59*, 12632–12640.

(2) Wang, H.-F.; Gan, W.; Lu, R.; Rao, Y.; Wu, B.-H. *Int. Rev. Phys. Chem.* **2005**, *24*, 191–256.

(3) Tong, Y.; Vila Verde, A.; Campen, R. K. *J. Phys. Chem. B* **2013**, *117*, 11753–11764.

(4) Liu, W.-T.; Shen, Y. R. *Phys. Rev. B* **2008**, *78*, 024302.

(5) Zelsmann, H. R. *J. Molec. Struct.* **1995**, *350*, 95–114.

(6) Sovago, M.; Campen, R. K.; Wurpel, G. W. H.; Müller, M.; Bakker, H. J.; Bonn, M. *Phys. Rev. Lett.* **2008**, *100*, 173901.

(7) Nagata, Y.; Hsieh, C.-S.; Hasegawa, T.; Voll, J.; Backus, E. H. G.; Bonn, M. *J. Phys. Chem. Lett.* **2013**, 1872–1877.